Biophysical Journal Volume 73 July 1997 318–332

Influence of Static and Dynamic Bends on the Birefringence Decay Profile of RNA Helices: Brownian Dynamics Simulations

Martin Zacharias and Paul J. Hagerman
Department of Biochemistry and Molecular Genetics, University of Colorado Health Sciences Center, Denver, Colorado 80262 USA

ABSTRACT Bends in nucleic acid helices can be quantified in a transient electric birefringence (TEB) experiment from the ratio of the terminal decay times of the bent molecule and its fully duplex counterpart (τ-ratio method). The apparent bend angles can be extracted from the experimental τ-ratios through the application of static (equilibrium-ensemble) hydrodynamic models; however, such models do not properly address the faster component(s) of the birefringence decay profile, which can represent up to 80% of the total birefringence signal for large bend angles. To address this latter issue, the relative amplitudes of the components in the birefringence decay profile have been analyzed through a series of Brownian dynamics (BD) simulations. Decay profiles have been simulated for three-, five-, and nine-bead models representing RNA molecules with central bends of 30°, 60°, and 90°, and with various degrees of associated angle dispersion. The BD simulations are in close agreement with experimental results for the fractional amplitudes, suggesting that both amplitudes and terminal τ-ratios can be used as a measure of the magnitudes of bends in the helix axis. Although the current results indicate that it is generally not possible to distinguish between relatively fixed and highly flexible bends from single τ-ratio measurements, because they can lead to similar reductions in terminal decay time and amplitude, measurements of the dependence of the fractional amplitudes on helix length may afford such a distinction.

INTRODUCTION

The quantitative characterization of the global geometries and flexibilities of simple, nonhelix structural elements in RNA and DNA is an important prerequisite for an understanding of both their individual biological roles and their participation in the formation of higher order structure. To this end, transient electric birefringence (TEB) has proved to be a useful tool (e.g., Hagerman, 1996), because the method is capable of providing precise estimates of the rotational diffusion constants for relatively short (~100–200 bp) nucleic acid helices that either possess or lack centrally placed nonhelix elements.

In the preceding investigation (Vacano and Hagerman, 1997) it was demonstrated that a particular form of the TEB method, the τ-ratio approach, is capable of quantifying the apparent angles—and in some instances, the angle dispersions—introduced between flanking helices by various nonhelix elements (e.g., bulges, loops, branches, etc.). The τ-ratio approach has typically relied on a comparison of the terminal (slow) decay times for linear and element-containing helices, where the ratio of the decay times is related to the bend angle through a Monte Carlo analysis of the (static) ensemble-averaged decay times of bent versus nonbent hydrodynamic chains. Although the use of the static model is both rapid and quantitatively valid, it is not applicable for modeling the faster component(s) in the birefringence decay profile. Because these faster components comprise up to 80% of the total birefringence amplitude as the bend angles approach 90° (Friederich et al., 1995; Zacharias and Hagerman, 1995a,b), substantial information pertaining to both helix conformation and dynamics is being lost if the interpretation of the decay profiles is restricted to the terminal decay times.

Therefore, in an effort to develop a more complete, quantitative picture of the decay profile for helices possessing centrally located bends, corresponding bead representations will be examined using dynamics approaches. The current analysis utilizes Brownian dynamics simulations for RNA helices that include both intrinsic flexibility and hydrodynamic interactions, and generally follows the earlier analysis by Allison and Nambi (1992), except for the addition of central bends that are either fixed, or which possess increased flexibility relative to the surrounding helix. It is demonstrated that the relative amplitudes are sensitive not only to the bend angle per se, but also to the intrinsic flexibility of the helix, although the distinction between stable and dispersive angles is surprisingly subtle. The angle-dependent amplitudes derived from the current Brownian dynamics analysis are in close agreement with the experimental amplitude-angle relationship for a series of RNA bulges (Zacharias and Hagerman, 1995a), suggesting that relatively simple dynamics models are capable of quantitatively representing the birefringence response of nucleic acids possessing elements of tertiary structure.

THEORETICAL BACKGROUND

Birefringence decay of a rigid body

In an effort to gain an understanding of the origin of the birefringence decay profile and, in particular, the relative

Received for publication 13 September 1996 and in final form 21 April 1997.

Address reprint requests to Dr. Paul J. Hagerman, Department of Biochemistry and Molecular Genetics, University of Colorado Health Sciences Center B-121, 4200 E. Ninth Avenue, Denver, CO 80262. Tel.: 303-315-8305; Fax: 303-315-5467; E-mail: paul.hagerman@uchsc.edu.

Dr. Zacharias's present address is Max Delbrück Centrum Berlin, Robert Rössle Straße, 13122 Berlin; and Humboldt Universität Berlin, Institut für Biologie, Invalidenstraße 42, 10115 Berlin.

0006-3495/97/07/318/15 $2.00

amplitudes of the individual exponential components, it is instructive to consider the birefringence decay of a rigid body (Wegener et al., 1979). The diffusional motion of a rigid body is conveniently described in a coordinate frame determined by the three principal components of the rotational diffusion tensor. The optical polarizability of a molecule in this principal (diffusion) frame can be described by a symmetrical, second-rank tensor. The overall polarizability of an ensemble of molecules in solution at any time is then given as the average over all orientations of the molecules, resulting in an (average) optical polarizability tensor of the solution in the laboratory frame. The difference between the solution polarizabilities, α_{33} and α_{11} (average zz and xx tensor components in the laboratory frame, respectively, where the field $\mathbf{E} = E\hat{x}$), averaged over all molecules in the solution, characterizes the solution birefringence. Finally, the probability of finding a molecule in a certain alignment with respect to the axis of orientational asymmetry (the field direction) is given (as a low-field approximation) by the product of an alignment tensor and the square of the applied field strength. This expression arises from a Taylor expansion of the Boltzmann probability for any orientation of the molecules in the electric field (to second order in E). The elements of the alignment tensor are determined by the electric polarizability tensor as well as products of components (dyadic tensor) of a possible permanent dipole moment of the molecule.

In their rigid-body analysis, Wegener et al. (1979) demonstrated that the general solution of the diffusion equation (in spherical coordinates) gives rise to the expression

$$\Delta\alpha(t)/E^2 = C \sum_{i=-2}^{+2} O_i I_i \exp(-t/\tau_i) \qquad (1)$$

for the field-free decay of birefringence ($\Delta\alpha$) following transient alignment in an external field (E). This expression possesses up to five exponential terms, which reflects the fact that symmetrical, second-rank tensors (the diffusion, optical polarizability, and alignment tensors) in spherical coordinates possess five independent components, which are linear combinations of the Cartesian components (Rose, 1957; Wegener et al., 1979). (Although symmetrical second-rank tensors possess up to six distinct elements, the trace of the tensor is invariant under rotation; thus there is a maximum of five independent components.) The analysis of Wegener et al. (1979) is particularly noteworthy for its demonstration that the amplitudes, O_iI_i, associated with each exponential term are products of separable contributions of the alignment tensor (I_i terms) and the optical polarizability tensor (O_i terms), at least to order E^2. Furthermore, Wegener et al. (1979) demonstrated that the slowest ($i = 0$) and fastest ($i = 2$) decay components were the only terms whose amplitudes contained only diagonal elements of the optical polarizability and alignment tensors; the other three components ($i = -2, -1, 1$) are given by products of off-diagonal tensor elements. Wegener's result has extremely important consequences for the study of birefringence decay. Specifically, for any structure that possesses sufficient symmetry for the optical polarizability and alignment tensors to be (approximately) diagonal in the principal (diffusion) frame, the decay profile will possess only two exponential components with nonzero amplitude: the fastest and the slowest.

More recently, Wegener (1986) analyzed the specific case of a centrally bent rod, modeled as a collection of 20 hydrodynamic centers; the analysis incorporated intrachain hydrodynamic interactions and considered various orienting mechanisms. Wegener concluded that the field-free birefringence decay profiles possess, at most, two exponentials. In this regard, for symmetrical, once-bent RNA helices, two-exponential decay profiles are observed almost exclusively (e.g., Zacharias and Hagerman, 1995a,b), suggesting that intrinsic flexibility, if it does not substantially destroy the symmetry of the molecule, will preserve the two-exponential profile. Furthermore, the fact that three of the amplitude terms are determined by products of off-diagonal tensor elements suggests that substantial molecular asymmetry may be tolerated before these latter amplitudes would become significant. This issue is currently being investigated separately.

The flexible, three-bead (trumbell) dynamical model

Roitman and Zimm (1984a,b; Roitman, 1984) have provided a solution for the dynamics of birefringence decay for a three-bead "trumbell" model in which intrinsic flexibility is introduced through a harmonic, interbead bending potential, $\varphi(\theta) = \epsilon\theta^2/2$, where θ is the bend angle ($\theta = \chi - \pi$ of Roitman and Zimm, 1984a,b, consider χ is the angle between the connecting segments and π (radians) represents the colinear arrangement of the two segments) between the two segments connecting the two outer beads to the central bead (bend vertex), and where ϵ is a spring force constant. The associated Boltzmann factor for a given angle is $\exp(-Z\theta^2)$, where $Z = \epsilon/2kT$. The trumbell model also provides for the inclusion of stable bends (θ_o in the current terminology), where $\varphi(\theta) = \epsilon(\theta - \theta_o)^2/2$. The model does not include hydrodynamic interactions among the beads; however, neglect of the latter is probably not serious, because Mellado et al. (1988) found only a small (~10%) change in the slow decay time upon removal of hydrodynamic interactions for a two-subunit structure connected by a flexible hinge. The numerical solution of the diffusion equation for this system indicates that the inclusion of flexibility will lead to a significant (fast) birefringence decay component (~10%) for linear molecules in the size range of the persistence length of the chain. Furthermore, the model predicts that even moderate bends (45°) will lead to a substantial decrease in the amplitude of the slow decay component, in contrast to the prediction of the rigid-rod model (Wegener et al., 1979) (see Fig. 1).

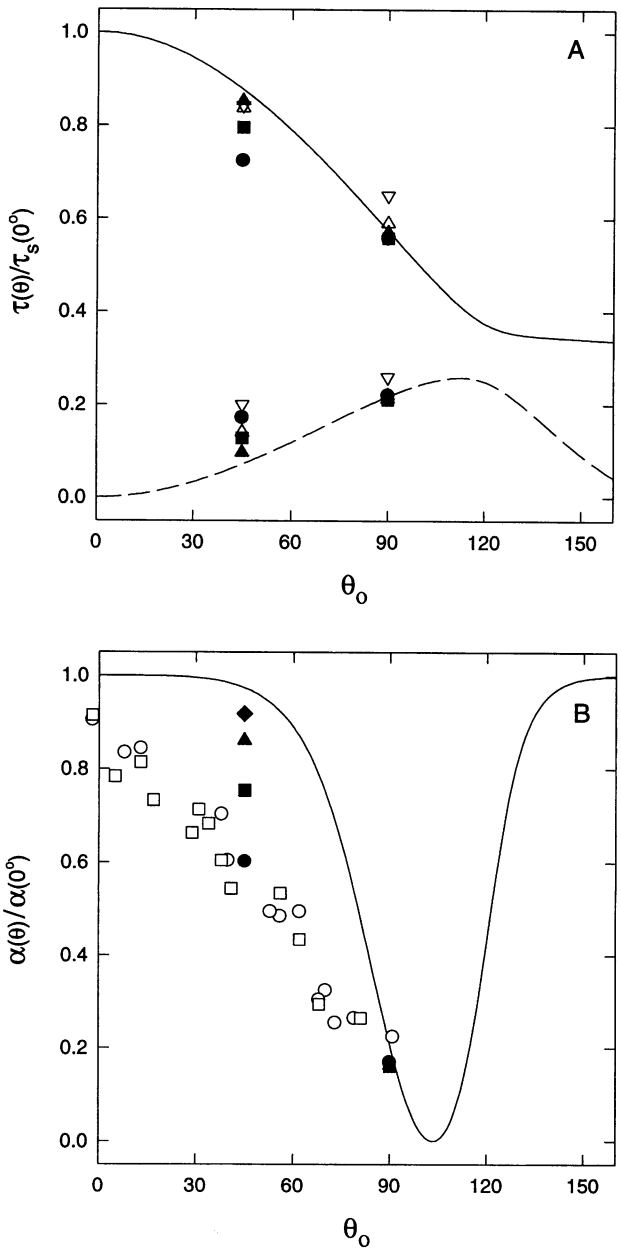

FIGURE 1 (*A*) Slow (s) (——) and fast (– – –) birefringence decay time constants, τ, and (*B*) relative (fractional) slow (——) decay amplitudes, α, for a rigid, three-bead model as a function of the stable bend angle, θ_0 (degrees). The decay times and amplitudes were computed using the rigid-body expressions of Wegener et al. (1979). Both fast and slow time constants are normalized to the slow decay time constant of the three-bead model lacking a stable bend; the slow amplitude component is normalized in an analogous fashion. For comparison, time constants and amplitudes for the dynamic three-bead (trumbell) model (Roitman and Zimm, 1984a,b; Roitman, 1984) are displayed for various effective helix rigidities: $Z = 4$ (▲), 2 (■), 1 (●), relative to a "linear" helix with $Z = 4$ (representing added bend dispersion); $Z = 2$ (△), 1 (▽), relative to "linear" helices with $Z = 2$ or 1, respectively (no added bend dispersion). For point of reference, the three-bead model with $Z \approx 1.3$–1.4 provides an approximate hydrodynamic representation of a 150-bp RNA with a persistence length of 700 Å. In *B*, $Z \cong 8$ (◆); the open symbols indicate the experimentally derived amplitudes for RNA helices possessing central bulges of specified (apparent) bend angle. □, Presence of Mg^{2+} ions; ○, absence of Mg^{2+} ions (Zacharias and Hagerman, 1995a,b).

Two features of the trumbell model should be noted. First, starting from the assumption of symmetry (i.e., a common principal coordinate frame) for the three tensors, Roitman and Zimm (1984b; Roitman, 1984) demonstrated that the inclusion of either flexibility or stable bends (or both) essentially preserves the two-exponential character of the decay profile, with additional, fast components comprising less than 3% of the total amplitude. Furthermore, although representing linear or bent DNA or RNA helices by only three hydrodynamic centers, the decay time and amplitude behavior of the trumbell (Roitman, 1984) is strikingly similar to that of experimental decay curves for RNA molecules possessing central bends (Gast et al., 1994; Amiri and Hagerman, 1994; Zacharias and Hagerman, 1995a,b; Friederich et al., 1995).

Brownian dynamics models for birefringence decay

The direct numerical solution of the diffusion equation for models comprising more than three beads represents a daunting task, particularly if hydrodynamic interactions and intrinsic flexibility are to be included. However, an alternative dynamical approach exists for the determination of the birefringence decay profile. This latter approach involves the computation of the phase-space trajectories of each chain by solving numerically the Langevin equation of motion in the diffusion (Brownian motion) regime (Ermak and McCammon, 1978; Fixman, 1978a,b). The time evolution of the *N*-bead probability distribution function, or of some other time-dependent physical characteristic (e.g., birefringence, light-scattering, etc.), can be obtained by taking the appropriate ensemble averages over the computed trajectories.

Brownian dynamics simulations have been used in a number of studies of enzyme-substrate encounters (Northrup et al., 1984; Sharp et al., 1987; Luty et al., 1993; Antosiewicz and McCammon, 1995), the dynamics of supercoiled DNA (Chirico and Langowski, 1994), and the reorientational dynamics of DNA upon application of electric fields (Grycuk et al., 1994). The approach has also been used extensively by Allison and co-workers (Allison and McCammon, 1984; Lewis et al., 1988; Allison and Nambi, 1992) to analyze the birefringence (and dichroism) decay profiles of bead representations of linear DNA.

The Brownian dynamics simulations of linear (flexible) chains have yielded several important results that bear on the current investigation:

1. Simulations of linear DNA helices in the size range 194–367 bp yield amplitudes of 10–15% for the fast component, in good agreement with experiment (Stellwagen, 1981; Hagerman, 1981; Elias and Eden, 1981; Diekmann et al., 1982).

2. Permanent and induced dipole orienting mechanisms result in essentially identical decay behavior; that is, the decay profile is independent of the orienting mechanism for relatively low fields.

3. Static (equilibrium-ensemble) models provide essentially quantitative agreement with the dynamics simulations for the terminal decay times, particularly in the τ-ratio mode (Vacano and Hagerman, 1997), even for dynamics models comprising as few as three beads.

4. Although dynamics models possessing only a small number of beads are capable of accurately representing the relative amplitudes of the slow and fast components of the decay profile, between 5 and 10 beads are necessary for the accurate representation of the faster decay time (Allison and Nambi, 1992).

METHODS

Brownian dynamics simulations and data analysis

Brownian dynamics simulations were performed using a procedure similar to the one described by Allison and Nambi (1992). For the simulations described in the current work, individual RNA molecules are represented by a chain of N beads (N = 3, 5, or 9), the centers of which are connected by $N - 1$ bonds. The reference bond length for a given chain is specified as the contour length of the RNA molecule divided by the number of bonds. During the course of the simulations, the bonds were constrained to their preset values by using an iterative constraint-satisfaction algorithm, SHAKE (Ryckaert et al., 1977), or were subject to a harmonic bond-stretching potential about the reference bond length. Dynamic chain flexibility was introduced through harmonic bending potentials between adjacent bonds (i.e., bending vertices at the bead centers); additional static and/or dynamic bending was introduced at the central bead angle. The bending potentials were assumed to be isotropic, with no distinction made between roll and tilt bending. Random starting chain configurations were generated as a Boltzmann ensemble, using Monte Carlo methods.

The Ermak-McCammon method (Ermak and McCammon, 1978) was used to solve the Langevin equation of motion,

$$\vec{r}_i(t + \Delta t) = \vec{r}_i(t) + \frac{1}{kT}\sum_j \tilde{D}_{ij} \cdot \vec{F}_j \cdot \Delta t + \vec{R}_i(\Delta t) \qquad (2)$$

where $\vec{r}_i(t)$ and $\vec{r}_i(t + \Delta t)$ are the positions of bead i before and after time step Δt; $\vec{F}_j$ is the force acting on bead j due to the harmonic bond stretching and bending potentials between beads; $\tilde{D}_{ij}$ is the diffusion tensor (see below); $\vec{R}_i(\Delta t)$ is a Gaussian random vector obtained from Gaussian random numbers (IMSL subroutine, GGNSM; IMSL, 1980), with deviates weighted by the elements of the hydrodynamic interaction tensor (Ermak and McCammon, 1978); and k and T are the Boltzmann constant and temperature (°K), respectively. T was set to 277°K (4°C) in the BD simulations, the same temperature that was used in our experimental birefringence decay measurements. Hydrodynamic interactions among the beads were computed from the Rotne-Prager (3 × 3) tensor of the bead system for nonoverlapping beads (Rotne and Prager, 1969), with

$$\tilde{D}_{ii} = kT/(6\pi\eta_o\sigma)\tilde{I} \qquad (3)$$

for bead i, and

$$\tilde{D}_{ij} = kT(8\pi\eta_o r_{ij})^{-1}\left[\left(\tilde{I} + \frac{\vec{r}_{ij}:\vec{r}_{ij}}{r_{ij}^2}\right) + \frac{2\sigma^2}{r_{ij}^2}\left(\frac{1}{3}\tilde{I} - \frac{\vec{r}_{ij}:\vec{r}_{ij}}{r_{ij}^2}\right)\right] \qquad (4)$$

for $j \neq i$, where σ is the hydrodynamic bead radius, $\vec{r}_{ij}$ and r_{ij} are the vectorial and scalar separations between beads i and j, $\tilde{I}$ is the unit tensor, $\vec{r}_{ij}:\vec{r}_{ij}$ is the dyadic product of the corresponding interbead vector, and η_o is the macroscopic (water) viscosity.

Parameterization of the bending force constants and bead diameters for the linear control molecule with uniform persistence length was performed by comparing ensemble-averaged diffusion constants for the N-bead models (N = 3, 5, or 9) with the corresponding "virtually" touching bead model described in the previous article (Vacano and Hagerman, 1997). The bead diameter for each Brownian dynamics model was adjusted to yield ensemble-averaged (three) principal diffusion coefficients and longest ensemble-averaged birefringence decay time constant that were equal (within 5%) to the corresponding values for the touching-bead model. For a 150-bp RNA (p = 700 Å), the above procedure yielded a bead radius of 20 Å for the five-bead model, and a radius of 17 Å for the nine-bead model. The touching-bead model itself comprises 14 beads with a hydrodynamic bead radius of 15.25 Å. For the three-bead model, no value for the bead diameter could be found that satisfies all of the above conditions; therefore, a bead radius (24.5 Å) was used that yields the same terminal (longest) birefringence decay constant as the touching-bead model. For the Brownian dynamics simulations of chains representing linear duplex RNA, the bending force constants were chosen to yield an rms end-to-end distance, $\langle r_{1N}^2\rangle^{1/2}$, that is equal to the expected end-to-end distance, $\langle r^2\rangle^{1/2}$. For a chain of length L and persistence length P, the latter quantity was obtained from the expression

$$\langle r^2\rangle/L^2 = (2P/L)[1 - P/L + (P/L)\exp(-L/P)] \qquad (5)$$

(Bloomfield et al., 1974). The central bend angle and the force constant for the central harmonic bending potential were systematically varied in different ensembles of BD simulations to obtain the functional dependence of the time constants and amplitudes on those parameters.

The normalized birefringence decay curves were computed from the ensemble averages of the following expression:

$$\begin{aligned}\Delta n(t)/\Delta n(0) &= C\sum_i\sum_j P_2[\hat{b}_i(t_0)\cdot\hat{b}_j(t_0 + t)] \\ &= C\sum_i\sum_j\left\{\frac{3}{2}\cos^2[b_i(t_0), b_j(t_0 + t)] - \frac{1}{2}\right\}\end{aligned} \qquad (6)$$

where C is a normalization constant, and where the $\hat{b}_i$ are unit bond vectors (Allison and Nambi, 1992). Thus the double sum is taken over the second Legendre polynomial (P_2) of the cosine of the angle between bead bond i at time t_0 and bead bond j at time $t_0 + t$ (for all bond pairs). The $\cos^2$ term in the second Legendre polynomial corresponds to an Euler transformation of the polarization component along a bond vector, j, at time t and an initial orientation of bond vector i, where the Euler transformation is specified by the angle between the two bonds. It should be noted that the functional form of the double sum (above) assumes an induced-dipole orienting mechanism with an E^2 or E^4 field dependence (Allison and Nambi, 1992). Allison and Nambi (1992) noted that there were no significant differences between the decay characteristics for the simulated ensembles using pure induced or permanent dipole-orienting mechanisms for linear DNA. However, in his study of rigid bent rods, Wegener (1986) found that the relative amplitudes (but not the time constants) of the birefringence decay profiles were dependent on the orienting mechanism (pure or mixed dipole character), particularly for large bend angles. Thus, with respect to relative amplitude, the current results are valid only for the induced dipole case, or where the influence of permanent dipoles on orientation is small. For the decay times, however, it is sufficient to demonstrate that the experimental birefringence decay profiles become independent of field strength for sufficiently low E; precise knowledge of the orienting mechanism is not required. This (experimental) criterion has the added advantage of ruling out field-induced distortions of the molecule under study, an assumption that is implicit in the simulations.

The ensemble average, $\langle \Delta n(t)/\Delta n(0) \rangle$, was accumulated at each time step, Δt, by pointwise averaging over 1000–10,000 trajectories per ensemble. The time step was varied between 0.31 ns and 2.5 ns, with no significant differences (less than 5%) noted in the bend-angle distribution functions or in the slow decay time constants and amplitudes for ensembles of simulations. Accordingly, time steps of 2.0 ns (three-bead model) or 1.0 ns (five- and nine-bead models) were used for most simulations. The fast decay time constant was not analyzed in detail, because its value is influenced significantly by both the step time and the data reduction process (see below). Each trajectory was recorded after a period of equilibration (500–1500 time steps) and was extended out to 12–15 μs. The computation of one trajectory for the three-, five-, and nine-bead models required 1.9, 4.5, and 11 s of CPU time, respectively, on an Indigo Extreme workstation (R8000 processor; Silicon Graphics). The ensemble-average birefringence decay curves were reduced to 40–500 points through window averaging, and were subsequently fit to a double-exponential decay function by the Levenberg-Marquardt (LM) method (Press et al., 1992) in essentially the same fashion as for the analysis of experimental TEB decay curves (e.g., Zacharias and Hagerman, 1995a,b, 1996), thus affording a direct comparison between the results of (BD) simulation and experiment. Finally, the use of a harmonic bond stretching potential instead of a fixed-length constraint, thus allowing a ~5% variation in the bond length during the BD runs, resulted in insignificant (<5%) alterations in the decay times.

The statistical error for the slow decay times and slow (fractional) amplitudes, estimated from independent ensembles (each comprising 5000–10,000 trajectories), was ~5% for stable bend angles of 0° and 30°, and approached 10% for the larger angles (60° and 90°). Although it is known from the numerical solutions of the diffusion equation of the three-bead "trumbell" model that the birefringence decay can contain more than two exponentials (Roitman and Zimm, 1984a,b), the additional components make up less than ~3% of the total decay amplitude. Moreover, whereas additional decay components have been reported for longer DNA molecules (e.g., 367 bp; Lewis et al., 1988), additional components have not been observed for RNA molecules shorter than ~200 bp (Gast et al., 1994; Zacharias and Hagerman, 1995a,b; Friederich et al., 1995; Amiri and Hagerman, 1994, 1996). The addition of a third exponential term to either the experimental or BD simulation results (this work) did not reduce the χ^2 statistic significantly in the LM analysis.

RESULTS

The fractional amplitude of the slowest decay component is sensitive to both the mean and the dispersion of the bend angle

In studying the birefringence response of nucleic acid helices that possess both intrinsic flexibility and central bends (possibly with additional flexibility), it is important to begin with a consideration of the field-free decay profile of a rigid, bent rod, because certain properties (e.g., large fast decay component) previously ascribed to flexibility or heterogeneity are, in fact, expected for the rigid system. Intrinsic and/or bend-associated flexibility can then be introduced to gauge the sensitivity of the various decay parameters to flexibility per se. The decay parameters for the rigid, symmetrical system are displayed in Fig. 1 and are based on the expressions provided in tables 1 and 3 of Wegener et al. (1979). (The equals sign in the third line of the expression for O_oI_o in Wegener et al. (1979) is a typographical error; it should be a plus.) An initial view of the influence of flexibility (chain dynamics) on the decay times and amplitudes is also displayed in Fig. 1 and follows directly from table 1 of Roitman and Zimm (1984b) and table 3 of Roitman (1984) for the elastic hinge (trumbell) model (Roitman and Zimm, 1984a).

Inspection of Fig. 1 *A* reveals that the introduction of intrinsic chain flexibility has very little effect on the angle-dependent τ-ratio for the slowest decay time, as expected from previous work (Zacharias and Hagerman, 1995a; Vacano and Hagerman, 1997). Moreover, although the presence of additional flexibility at the bend results in a reduction in the terminal τ-ratio for a bend of 45°, added

flexibility has very little effect on the τ-ratio for the 90° bend (Roitman, 1984). Thus, although a single (terminal) τ-ratio is a sensitive measure of the apparent (mean) angle of a central bend (Vacano and Hagerman, 1997), such τ-ratios, by themselves, provide only limited information on bend-angle dispersion, particularly for bends approaching 90°. In other words, the reduction in τ-ratio at 45°, due to added bend dispersion, is not distinguishable from a more rigid bend in the vicinity of 70–80°. However, as discussed in the preceding paper (Vacano and Hagerman, 1997), τ-ratio information can be used to set bounds on the added angle dispersion. One fares little better when considering the faster decay component, because the slowing of that component (e.g., at 45°) is again approximately equivalent to a more static bend of larger angle (Fig. 1 *A*), both situations reflecting a greater departure of the chain configuration from linearity, and hence a larger frictional component about the principal axis of asymmetry. However, the analysis of Roitman (1984) does indicate that additional (small amplitude) fast components may appear for larger bend angles, and that such components may depend strongly on the internal chain dynamics.

One significant advantage of the incorporation of chain dynamics into the analysis of birefringence decay is the ability to study the amplitude behavior for the various decay components (Roitman, 1984; Roitman and Zimm, 1984a,b; Lewis et al., 1988; Allison and Nambi, 1992). Again, one can use the amplitudes of Wegener et al. (1979) as a point of departure in considering the effects of additional bend-associated flexibility (Fig. 1 *B*). In this instance, the analysis of Roitman (1984; Roitman and Zimm, 1984a,b) indicates that the addition of either intrinsic or bend-associated flexibility results in a striking reduction in the fractional amplitude of the terminal decay component; again, such effects are most pronounced for apparent angles that are far removed from 90°.

Superimposed on the computational results are experimental data for bulge-induced bends in RNA (Zacharias and Hagerman, 1995a). It is evident that the data are incompatible with a rigid helix; however, the data are consistent with the known flexibility of RNA (≈ 700 Å) (Gast and Hagerman, 1991; Kebbekus et al., 1995) in the absence of any substantial (additional) bend-associated flexibility. As expected, the experimental data fall close to the limiting curve for the rigid helix (or flexible elastic hinge model) at 90°. Thus, at least at the level of the three-bead dynamics representation of a flexible chain (Roitman, 1984; Roitman and Zimm, 1984a,b), the effects of additional bend-angle dispersion in the vicinity of 90° are particularly subtle. It is encouraging that even a relatively simple (three-bead) representation can reproduce many of the features of the birefringence decay profile.

Finally, one can, in principle, use the variation in total birefringence amplitude with apparent angle as an independent means of gauging the combined contributions of intrinsic and bend-angle-associated flexibilities on chain distributions (Fig. 2). The analysis of Wegener et al. (1979; Wegener, 1986) can be used to estimate the angle-dependent variation for rigid as well as flexible chains, because the total birefringence effectively samples a rigid distribution of conformations (i.e., on the time scale of the interaction of light with the molecules). We use the expression

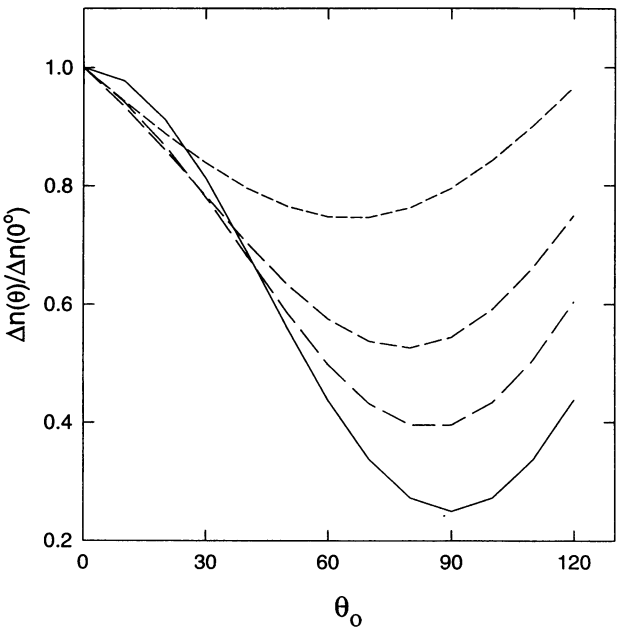

FIGURE 2 Analysis of the expected variation in total birefringence amplitude as a function of the stable bend angle and extent of angular dispersion for the three-bead model. Birefringence amplitudes, $\Delta n(\theta)$, are given by $O_0I_0 + O_2I_2$ (Wegener et al., 1979) as a function of θ_o and are normalized with respect to Δn at $\theta_o = 0$. For this example, the diagonal tensor components (Wegener et al., 1979) are given as $\alpha_{11} = \chi_{11} = \sin^2(\theta/2)$, and $\alpha_{33} = \cos^2(\theta/2)$; these values correspond to the rigid case. "Flexibility" is added as dispersion in θ according to the distribution function $P(\theta) = \sin(\theta)\exp[-Z(\theta - \theta_o)^2]$, with $\Delta n(\theta) = \int_\theta (O_0I_0 + O_2I_2)d\theta$. Plots are given for $Z = 8$ (——), 4 (— —), 2 (– – –), and 1 (- - - - -).

$$\Delta n(\theta)/\Delta n(0) = [O_0I_0(\theta) + O_2I_2(\theta)]/[O_0I_0(0) + O_2I_2(0)] \quad (7)$$

where the individual terms are given in table 3 of Wegener et al. (1979) (with correction, as noted above). For the purpose of illustration, we have used $\alpha_{33} = \cos^2(\theta/2)$, and $\alpha_{11} = \chi_{11} = \sin^2(\theta/2)$, where χ is the alignment tensor. Moreover, additional flexibility has been represented through the angle distribution function,

$$P(\theta) = C\sin(\theta)\exp[-Z(\theta - \theta_o)^2] \quad (8)$$

where $Z = \epsilon/2kT$ (Roitman and Zimm, 1984a). This analysis predicts a fourfold drop in signal (at 90°) relative to the 0° value for a rigid helix, in agreement with more recent results of Wegener (1986); however, as the helix becomes more flexible, the angle-dependent decrease is much less pronounced. Although this effect has not been explored experimentally in any detail, the observed drop in birefringence signal for RNA bends spanning the range of 0° to 90° is less

than ~30%, as expected for the RNA helix (Friederich and Hagerman, unpublished results).

The absence of any dependence of the decay times and fractional amplitudes on the strength of the orienting field defines an operational "low-field" criterion for comparing experimental and computed decay profiles for nucleic acid helices

Both static and dynamic representations of the birefringence decay profile assume "low-field," limiting behavior of the molecules being modeled (Wegener et al., 1979; Roitman and Zimm, 1984a,b; Allison and Nambi, 1992). In effect, this assumption implies that once the field is turned off, neither the structure nor the internal dynamics of the molecules are functions of the strength of the orienting field. Of course, the total birefringence amplitude will exhibit a strong field dependence, but this latter property simply reflects a greater net orientation—the normalized decay profile is assumed to be independent of changes in field strength for an induced-dipole orienting mechanism (see Introduction). In this regard, significant field-strength-dependent effects on fractional amplitudes and decay times have been observed for the electric dichroism decay profiles of small DNA fragments at high fields (Diekmann et al., 1982), and for the TEB decay profiles of larger DNA fragments at relatively low fields (Stellwagen, 1981; Elias and Eden, 1981; Hagerman, 1981; Lewis et al., 1986, 1988).

The computational studies cited above generally couch "low-field" behavior in terms of E^2 (Kerr law) behavior; that is, a low-field domain in which the total birefringence amplitude increases as the square of the strength of the orienting field. However, as discussed previously (Hagerman and Hagerman, 1996), the E^2 dependence is not necessarily the most appropriate criterion for low-field hydrodynamic behavior. In that investigation, it was demonstrated that decay times varied by less than 2% over a 30-fold range in field strength ($E \leq 10$ kV/cm), despite the fact that departures from Kerr law behavior were observed above 6–8 kV/cm. Indeed, we are unaware of any experimental or theoretical work that establishes Kerr law behavior as a sufficient (or necessary) criterion for low-field (limiting) hydrodynamic behavior. Moreover, we have observed that decay times and (fractional) amplitudes are independent of field strength ($E \leq 10$ kV/cm) for all RNA systems examined thus far (e.g., Shen and Hagerman, 1994; Zacharias and Hagerman, 1995a,b; Friederich et al., 1995; Amiri and Hagerman, 1996), despite observed departures from Kerr law behavior above 6–8 kV/cm (e.g., Fig. 3).

In view of the above, we would propose that a more appropriate operational criterion of low-field hydrodynamic behavior is the demonstrated absence of any dependence of the decay times or fractional amplitudes on the strength of the orienting field. Experimental demonstration of this criterion is sufficient for the purpose of comparing the experimental decay time and amplitude behavior to the low-field behavior predicted from computational (static or dynamic) models. Moreover, even under conditions where a field-strength-dependence of the fractional amplitudes is observed, as with longer, or more flexible molecules (Hagerman, 1981; Stellwagen, 1981; Elias and Eden, 1981; Diekmann et al., 1982), limiting (E-independent) behavior is apparent for the terminal decay time. However, it should be noted that the field independence of fractional amplitudes may not be a completely general result, even for small nucleic acids, because elements possessing substantial tertiary structure may be associated with some permanent dipole character; this issue merits further experimental study.

Brownian dynamics simulations provide an accurate representation of the birefringence decay profiles for RNA molecules that possess central bends

As discussed above, whereas the equilibrium-ensemble approach (Hagerman and Zimm, 1981) accurately represents the relationship between terminal τ-ratios for bent versus linear DNA or RNA molecules and the magnitude of the bend (Roitman, 1984), it is incapable of representing either the fractional amplitudes or the faster decay time for the decay profile. For this latter purpose, dynamical approaches must be employed. Therefore, to examine the influence of bends on the predicted decay curves, Brownian dynamics simulations were performed on a series of model chains comprising three, five, or nine beads, each representing a 150-bp RNA molecule that possesses either a fixed bend or a point of increased flexibility at its center.

Representative (computed) TEB decay curves for molecules possessing central bends of 0°, 30°, 60°, or 90° are displayed in Fig. 4, *A–C*, for each bead model. For comparison, a set of experimental decay curves is displayed (Fig. 4 *D*) for 148-bp RNA molecules that possess no bulge (0°; linear control duplex), a U_2 bulge (~40°), a U_4 bulge (~60°), or an A_6 bulge (~90°) (Zacharias and Hagerman, 1995a). As is evident from Fig. 4, the simulated decay curves display the same features as the experimental profiles; in particular, both experimental and simulated decay curves possess a characteristic double-exponential form. Furthermore, the τ-ratios (Fig. 5) and terminal (fractional) amplitudes (Fig. 6) decrease with increasing bend angle for all simulation (bead) models, as anticipated from the earlier dynamics analysis of Roitman (1984), and in close agreement with the experimental data for RNA bulges (Zacharias and Hagerman, 1995a,b). In considering the comparison between the experimental and computational systems, it should be noted that the experimentally derived bend angles for the bulges were estimated solely from the terminal τ-ratios on the basis of the equilibrium-ensemble approach (Zacharias and Hagerman, 1996; Vacano and Hagerman, 1997). Moreover, the simulated decay profiles for chains possessing bends are related to the experimental results solely through the configurational and hydrodynamic prop-

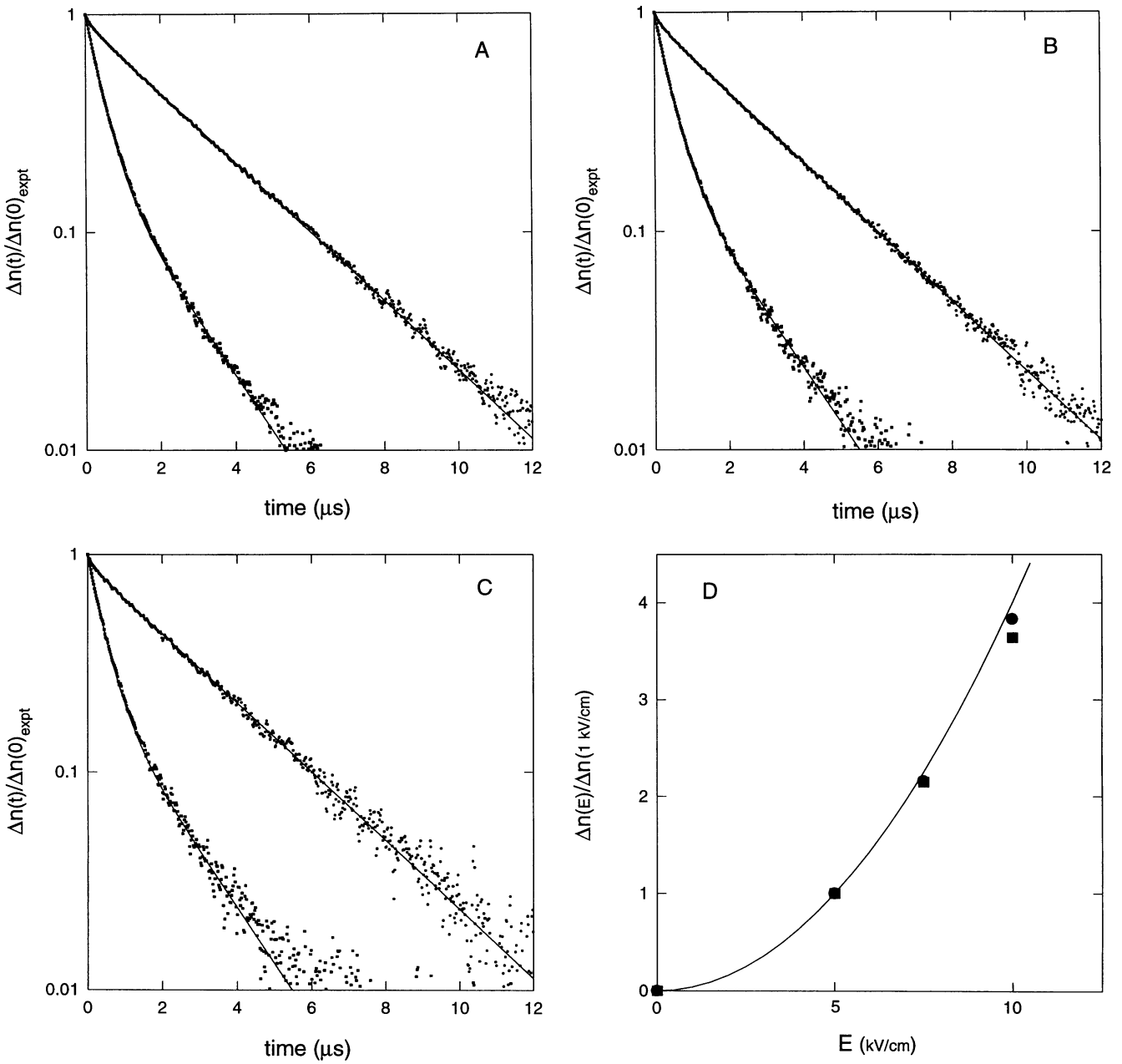

FIGURE 3 Absence of a field-strength dependence for experimental birefringence decay curves of bent RNA molecules. Decay curves (field off) are displayed in separate panels for several values of the orienting field (1.0-μs orienting pulse): (*A*) 10 kV/cm, (*B*) 7.5 kV/cm, (*C*) 5 kV/cm. Displayed in each panel are decay curves for a 148-bp linear duplex RNA molecule (●) and a heteroduplex construct (■) comprising the 148-bp duplex with an A_5 bulge at its center (Zacharias and Hagerman, 1995a,b). RNA concentration: ~0.13 μg/μl. Buffer: 5 mM $NaPO_4$, 0.125 mM NaEDTA, pH 7.2. Temperature: 4°C. The decay curves in *A* represent averages over 128 accumulated transients, whereas the curves in *B* and *C* are averages over 256 transients. Other experimental procedures are as described in Zacharias and Hagerman (1995a,b). Associated fast (f) and slow (s) decay times (τ, μs) and fractional slow amplitudes (α) are as follows:

Panel	Species	τ_f	τ_s	α
(A)	Duplex	0.28	2.74	0.90
	A_5	0.42	1.71	0.27
(B)	Duplex	0.26	2.73	0.90
	A_5	0.41	1.69	0.26
(C)	Duplex	0.26	2.75	0.89
	A_5	0.42	1.72	0.27

(*D*) Dependence of the total birefringence signal on the strength of the orienting field; the solid line represents a quadratic function (E^2 dependence).

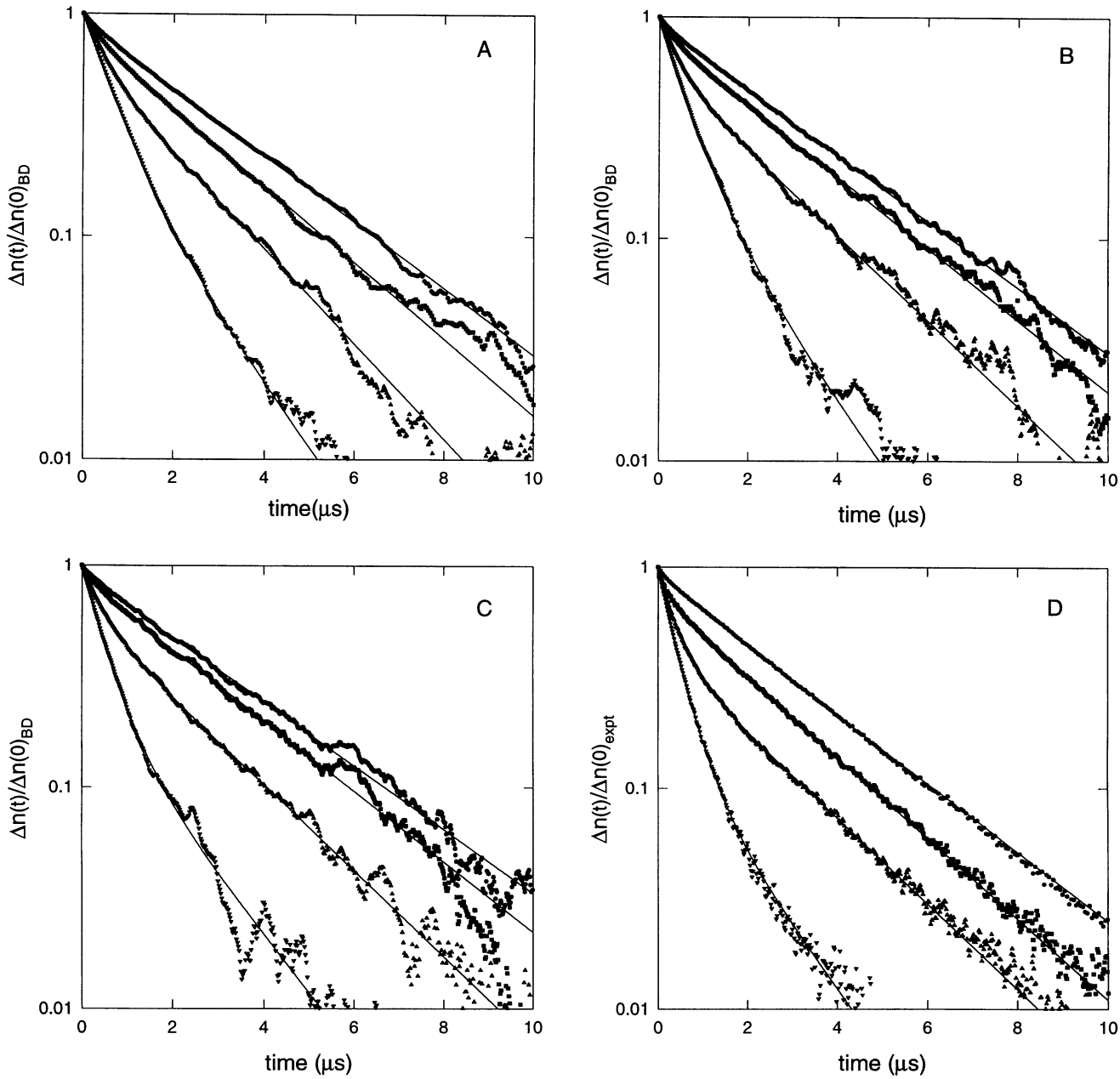

FIGURE 4 Representative birefringence decay curves from Brownian dynamics simulations of a 148-bp RNA molecule with a persistence length of 700 Å, and a central (stable) bend of 0° (linear control) (●), 30° (■), 60° (▲), or 90° (▼). The first three panels represent various *N*-bead models as follows: (*A*) three-bead, (*B*) five-bead, (*C*) nine-bead. Quantitative results for the curves displayed in parts *A–C*, averaged over several independent simulations, are given in Table 1. (*D*) Experimental decay curves corresponding to 0° (linear 148-bp RNA) (●), ~40° (U_2 bulge) (■), ~60° (U_4 bulge) (▲), and ~90° (A_6 bulge) (▼) (Zacharias and Hagerman, 1995a,b). The latter angles were estimated from an analysis of the terminal decay times (τ-ratio approach), using the equilibrium-ensemble method. Decay times and amplitudes for the curves in *D* are provided in table 2 (absence of Mg^{2+}) of Zacharias and Hagerman (1995a).

erties of the unbent molecules/chains, with no adjustable parameters for a model with a specified bend.

The most striking aspect of the Brownian dynamics simulations is the close agreement of the τ-ratios with the corresponding values derived from the equilibrium-ensemble approach (Fig. 5) (Vacano and Hagerman, 1997). This agreement supports the application of τ-ratio determinations using the latter approach, which is a much faster computational process. It should be noted that the important quantities in the Brownian dynamics analysis are not the absolute values of the slow and fast decay times and amplitudes, because such quantities can be adjusted for the linear species by small changes in bead radii; rather, quantities of interest are the decay time ratios (both between linear and

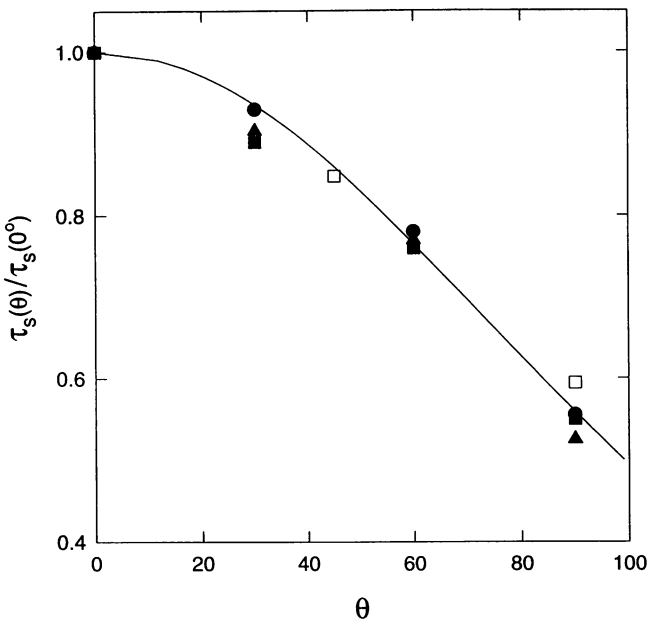

FIGURE 5 Dependence of the slow decay time on the central (stable) bend angle θ_o (degrees) for various hydrodynamic models, plotted as the ratio, $\tau_s(\theta)/\tau_s(0°)$, where $\tau_s(0°)$ corresponds to the (slow) computed decay time for the linear control. Brownian dynamics simulations: ■, three-bead; ●, five-bead; ▲, nine-bead; □, results from the analytical, dynamics (trumbell) model of Roitman and Zimm (1984a,b; Roitman, 1984). The solid line represents the corresponding τ-ratio computed using the equilibrium-ensemble method (equation 2 in Vacano and Hagerman, 1997). It should be noted that the solid line does not represent a fit to the symbols; once the properties of the RNA helix have been specified (L, 148 bp; P, 700 Å; rise, 2.8 Å/bp; hydrodynamic radius, 13 Å) for both dynamics and equilibrium-ensemble approaches, there are no independently adjustable parameters. This point applies as well to Figs. 7 and 9.

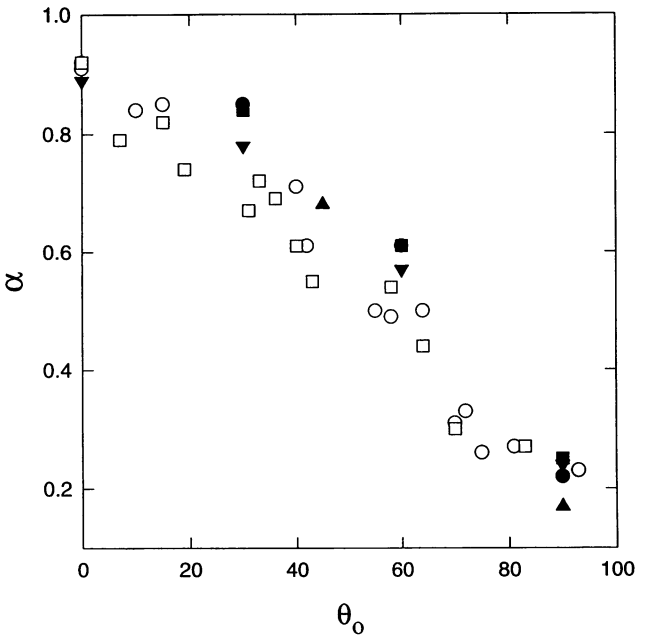

FIGURE 6 Amplitudes for the slow decay component, obtained from Brownian dynamics simulations. Models: ▼, three-bead; ■ five-bead; ●, nine-bead; ▲, trumbell model of Roitman and Zimm (1984a,b; Roitman, 1984). Corresponding experimental amplitudes are presented for RNA molecules that possess central A_n or U_n bulges. ○, Absence of Mg^{2+} ions; □, presence of Mg^{2+} ions (Zacharias and Hagerman, 1995a,b).

bent species, and between fast and slow phases) and the fractional amplitudes. Whereas the τ-ratios for the slow decay component in the Brownian dynamics simulations evidence remarkable agreement with the equilibrium-ensemble results, even for the three-bead case (Fig. 5), decay times for the fast component in the decay profile (relative to the slower decay time) are more accurately predicted by models containing more beads. This latter result is consistent with earlier Brownian dynamics simulations of linear DNA (Lewis et al., 1988; Allison and Nambi, 1992). Finally, it is evident from Fig. 4 (see also Table 1) that the simulated profile for the linear control (150-bp chain; P = 700 Å) is very similar to the experimental decay curves for a 148-bp dsRNA (τ_{slow}, 2.80 μs; τ_{fast}, 0.25 μs; α_{slow}, 0.91; Zacharias and Hagerman, 1995a).

It was noted earlier (Fig. 1 *B*) that the fractional amplitudes of bend-containing RNA molecules are much smaller than predicted on the basis of rigid-rod or bead models, but that even the simple, three-bead dynamics model (Roitman, 1984) yields reasonable agreement with the experimental results when intrinsic helix flexibility is taken into account. This amplitude behavior has been examined in more detail (Fig. 6, Table 1) for the Brownian dynamics models, and within the standard errors of the simulation results generally confirms the behavior predicted by Roitman (1984). Moreover, the simulated amplitudes generally lie quite close to the experimental values for the bulge series (Zacharias and Hagerman, 1995a), with simulated values slightly above the experimental values for angles in the 30°-60° range, and all in quantitative agreement for angles approaching 90°.

There are two additional aspects of the amplitude behavior that deserve comment. First, for angles in the 30°-60° range, there appears to be a slight trend to larger slow amplitudes for a given angle as the number of beads in the model increases from three to nine. Although this trend may well reflect the fact that larger numbers of beads provide a better representation of the experimental system, we cannot yet exclude small effects due to the increased level of non-Gaussian noise (1–5%) in the decay profiles for larger bead numbers (Fig. 4). Second, the small differences between the computed and experimental amplitudes may reflect residual uncertainties associated with the assignment of interbead angle variances based on the comparison of linear (experimental and computational) species, or the existence of a small reduction in intrinsic stiffness at the bulge for the experimental system. This latter issue will be addressed in the next section; however, the results presented in Fig. 6 demonstrate that the Brownian dynamics approach generally provides an excellent representation of the slow amplitude for bent helices.

TABLE 1 Averaged results of Brownian dynamics simulations for *N*-bead models possessing stable central bends*

	0°*			30°			60°			90°		
Model	τ_f	$\alpha^{\#}$	$\tau_s^{\S}$	τ_f	α	τ_s	τ_f	α	τ_s	τ_f	α	τ_s
3-bead	0.38	0.89	2.84	0.45	0.78	2.49	0.54	0.57	2.08	0.68	0.24	1.57
5-bead	0.22	0.92	2.86	0.31	0.84	2.64	0.44	0.61	2.25	0.55	0.25	1.60
9-bead	0.28	0.92	2.89	0.38	0.85	2.58	0.45	0.61	2.20	0.53	0.22	1.65

*Stable (central) bend angle, θ_o (degrees). The total angle at any given instant is the sum of the stable (specified) angle and the instantaneous angle due to thermal fluctuations (see Vacano and Hagerman, 1997).

#Fractional (slow) amplitude of the simulated birefringence decay profile; the relative amplitude associated with the fast phase is $1 - \alpha$.

§τ_f and τ_s are the time constants (μs) associated with the fast and slow decay components, respectively. Standard errors (expressed as % mean) for the slow decay times and amplitudes are ~5% for 0° and 30° angles, and 10% for 60° and 90° angles.

Analysis of the influence of additional flexibility at the site of bending

In the preceding sections, the results of static and Brownian dynamics computations were presented for *N*-bead models in which the central bends lack any additional flexibility (increased angle dispersion) over the intrinsic flexibility of the surrounding helix. However, it is generally not known a priori whether a particular nonhelix element is more flexible than its flanking helices. One approach to the issue of increased angle dispersion was presented in the preceding article (Vacano and Hagerman, 1997), in which it was demonstrated that multiple τ-ratio measurements, employing pairs of variably phased bends, could provide information regarding both lateral and torsional dispersion. However, the phasing method, which considers only the terminal decay times, is quite involved at the experimental level (Friederich et al., manuscript in preparation). An alternative approach, suggested by Fig. 1 *B*, would involve an analysis of the slow (fractional) amplitude, because this quantity is sensitive to the intrinsic flexibility of the molecules being evaluated, particularly for apparent angles that are less than ~80°.

Therefore, to examine the influence of additional angular dispersion on the birefringence decay profile, Brownian dynamics simulations have been performed for five-bead chains representing 150-bp RNA molecules, where the central bend is either stable (specified θ_o; $\langle\theta^2\rangle^{1/2}$ equal to that of the linear control) or purely dispersive ($\theta_o = 0°$, $\langle\theta^2\rangle^{1/2}$ equivalent to $\theta_o + \langle\theta^2\rangle^{1/2}_{linear}$). The results for this set of simulations are displayed in Fig. 7. It is evident that neither the τ-ratios nor the fractional amplitudes afford a clear distinction between fixed and dispersive bends; however, it will turn out that the similar decay profiles (τ-ratios and amplitudes) for the two types of bend are, to some extent, a result of the length of the molecules chosen for study. This last issue will be discussed below.

In addition, the characteristics of the birefringence decay profiles were examined for bends of mixed fixed and dispersive character. Five-bead models possessing central bends of 30°, 60°, and 90° were examined for various central bend angle force constants. The distribution functions for the central bend angles are displayed in Fig. 8. The major consequence of added dispersion is a shift in the peak of the distribution functions (and the rms angles) toward 90°, with the largest shifts occurring for the smallest angles. This result is entirely consistent with the results of a similar analysis using the equilibrium-ensemble approach (Vacano and Hagerman, 1997). It should be noted that for a fixed bend of 90°, there is a slight shift to smaller angles; this appears to be a consequence of self-exclusion for chains possessing the most acute bends.

The consequences of the shift in the distribution functions can be appreciated by examining the results of Brownian dynamics simulations for the cases represented in Fig. 8. When the τ-ratios and amplitudes are plotted for the values of the stable (specified) angles (Fig. 9, *A* and *C*, respectively), there is a significant spread of the ratios and amplitudes that is particularly pronounced for the 30° bend. This spread is a consequence of the dispersive character of the bends and, in particular, shifts in the angle distributions, as can be appreciated by replotting the dependent quantities versus the "corrected" bend angles, where $\theta_{corr} = \theta_o + \Delta\theta_{rms}$ (Fig. 9, *B* and *D*). Again, these results demonstrate that fixed and dispersive bends lead to very similar birefringence decay profiles, at least with respect to the terminal τ-ratios and amplitudes.

The similar behaviors of fixed and dispersive bends for RNA molecules in the 150–250-bp range can be understood by examining the bend angle distribution functions for a simple case, namely, the trumbell model. A comparison of the distribution functions for the central bend of the trumbell is provided in Fig. 10 for various values of the bending force constant (representing chains of different lengths). For a chain that is longer than the persistence length (e.g., $Z = 1.0$; corresponding to an RNA of ~200–250 bp), the fixed and dispersive angle distribution functions are quite similar to one another, although they clearly differ from the distribution function for the linear chain (Fig. 10 *A*). As a consequence, the decay profiles for stable and purely dispersive bends are nearly identical, an observation that reinforces the previous conclusion that the TEB experiment is responding to the distributional average properties of the ensemble (Roitman and Zimm, 1984b; Roitman, 1984).

However, for shorter (or stiffer) chains ($Z = 4$, rigid), the distributions for the fixed bends become much narrower than the distributions for the dispersive bends (Fig. 10, *B*

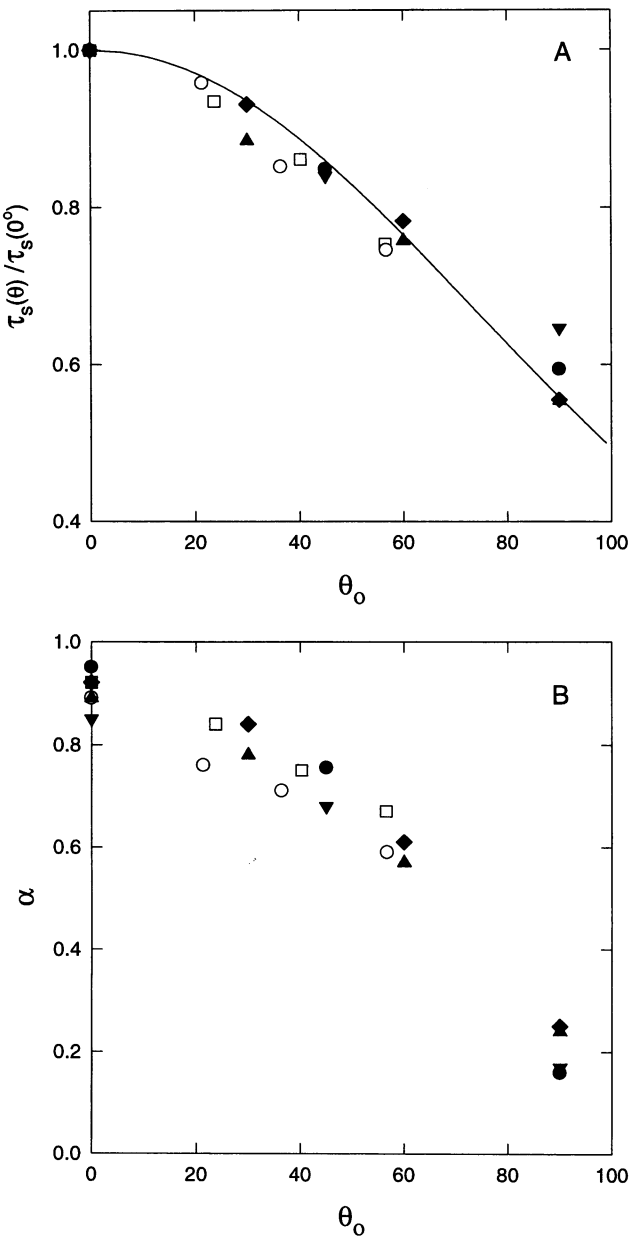

FIGURE 7 Dependence of the slow decay times (*A*) and amplitudes (*B*) of the birefringence decay profiles on the nature and magnitude of the central bend, for several computational models. Brownian dynamics simulations: ▲, three-bead, stable bend; ◆, five-bead, stable bend; ○, three-bead, pure increase in flexibility (dispersive bending); □, five-bead, dispersive bending. Trumbell model of Roitman and Zimm (1984a,b; Roitman, 1984): ▼, stable bend, $Z = 1.0$; ●, stable bend, $Z = 2.0$. Results of equilibrium-ensemble computations (equation 2 in Vacano and Hagerman, 1997) are also displayed in *A* (——). For dispersive bending, the additional rms dispersion is determined by the relation $\Delta\theta_{rms} = [\langle\theta^2\rangle - \langle\theta^2\rangle_{linear}]^{1/2}$, where $\langle\theta^2\rangle$ is the variance of the bend angle distribution for the model with increased central bond angle flexibility, and $\langle\theta^2\rangle_{linear}$ is the corresponding value for the linear control.

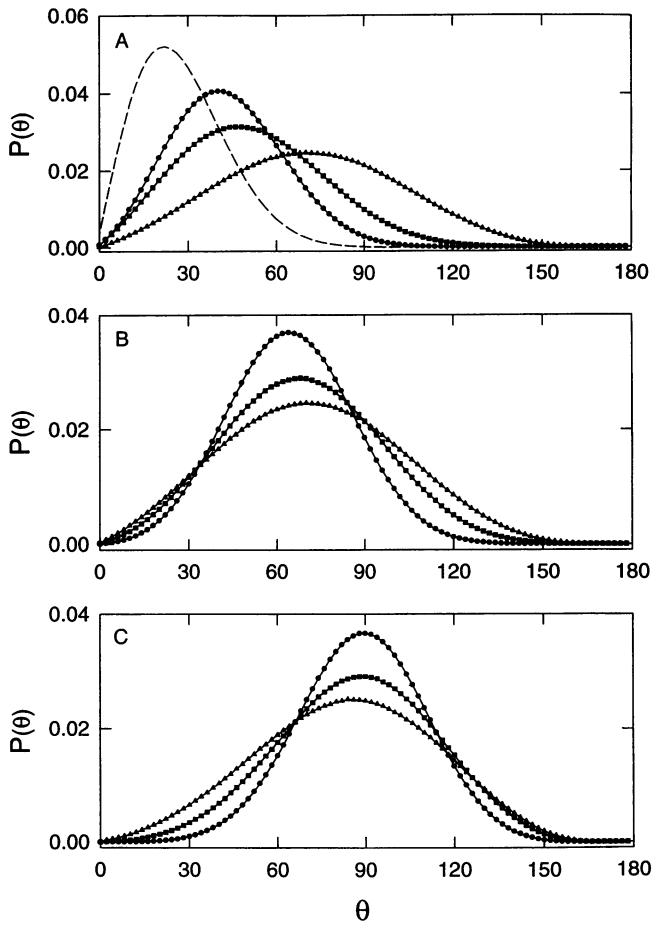

FIGURE 8 Distribution functions, $P(\theta)$, for the central bend angle (θ) of a five-bead model for various values of the stable bend and bending force constant. The distribution functions were obtained from Brownian dynamics simulations of chains with stable bends, θ_o, of 30° (*A*), 60° (*B*), or 90° (*C*). The central bend potential, $E(\theta) = k_a(\theta - \theta_o)^2$, is specified by a bending force constant, k_a, that is 1.0× (●), 0.5× (■), or 0.25× (▲) the force constant used to represent a linear chain with a persistence length of 700 Å; the distribution function for the latter is displayed in *A* (– – –).

and *C*), reflecting the loss of configurational dispersion from the rest of the chain (increasing *Z*). As a consequence, the fractional slow amplitudes diverge for the two cases (Fig. 10, *E* and *F*). For the case depicted in Fig. 10, the fractional amplitudes are nearly equal for $Z = 1$ (0.603, stable bend; 0.636, increased dispersion). However, as the helix becomes increasingly rigid (or shorter), the amplitude for the stable bend approaches 1.0, whereas the amplitude for the dispersive bend approaches 0.81, a difference of 19%, readily detectable with current TEB instrumentation (e.g., Amiri and Hagerman, 1996). Over the same range, the variation in the τ-ratios for the two cases is much smaller (~5%). Thus, although highly approximate, this analysis makes an interesting experimental prediction: for a given nonhelix element, the fractional slow amplitude will increase with decreasing fragment length, and in a manner that depends on whether the bend is stable or dispersive in character; whereas the apparent angle, itself derived from the τ-ratio, will experience relatively modest variation (see also Vacano and Hagerman, 1997).

The current Brownian dynamics analysis has not sought an accurate description of the fast decay time constant(s),

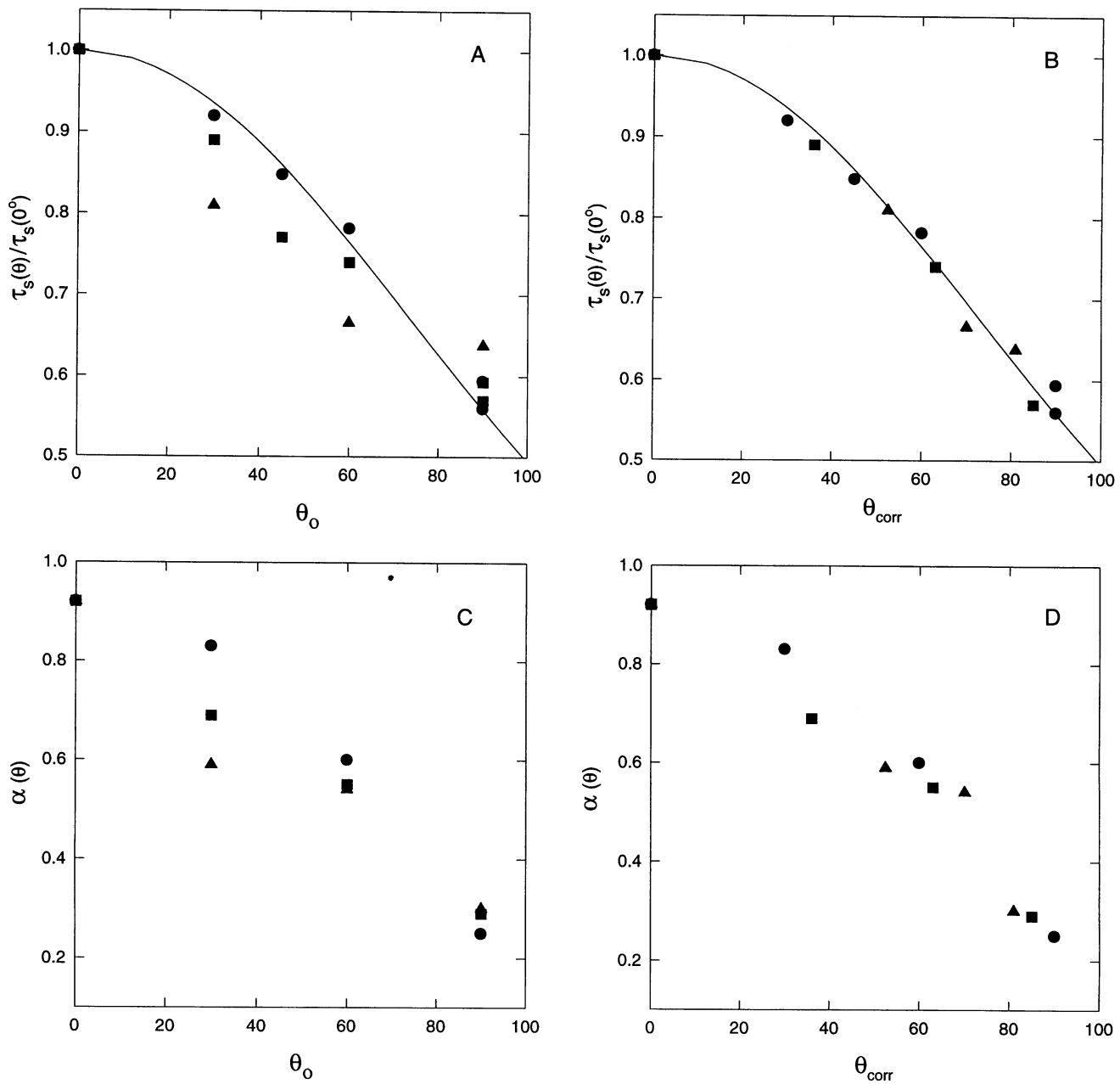

FIGURE 9 Computed τ-ratios and amplitudes for the slow component of the birefringence decay curves from Brownian dynamics simulations for a five-bead model with a central force constant that is 1.0× (●), 0.5× (■), or 0.25× (▲) the force constant used to represent the linear control (p = 700 Å; see Methods). The bending potential is specified in the legend to Fig. 8. (*A* and *C*) τ-ratios and amplitudes, respectively, plotted as a function of the specified (stable) angle, θ_o. (*B* and *D*) τ-ratios and amplitudes plotted as a function of a "corrected" angle, $\theta_{corr} = \theta_o + \Delta\theta$, where $\Delta\theta$ corresponds to the shift in the maximum of the bend angle distribution from θ_o due to the change in central flexibility (see Fig. 8).

even though the latter are expected to provide additional (and undoubtedly better) information pertaining to the flexibility of nonhelix elements. It is anticipated that the accurate simulation of the faster components will require additional beads, which is simply an issue of additional computational expenditure. However, such an analysis is clearly worth the effort, because the amplitude differences described above are relatively small, even for the extreme cases of purely dispersive and stable bends. Finally, whereas the TEB method provides a precise, quantitative means for determining the ensemble-averaged angles, other methods, such as time-resolved fluorescence resonance energy transfer (trFRET) (e.g., Eis and Millar, 1993), are particularly useful for the specific assessment of angle dispersion.

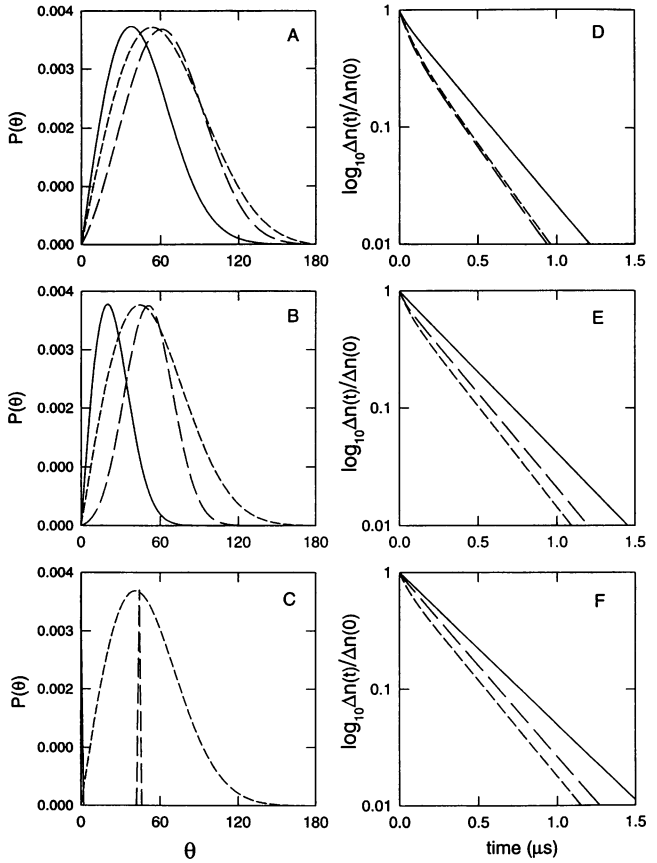

FIGURE 10 Bend angle distribution functions for a three-bead model representing either a linear RNA molecule (——), a molecule with a stable, central bend (θ_o) of 45° (— —), or a molecule with a purely dispersive bend ($\Delta\theta_{rms} = \langle\theta^2\rangle^{1/2}$) of 45° (– – –). The angle distribution functions are as follows: $P(\theta)_{linear} = C\sin(\theta)\exp[-Z\theta^2]$; $P(\theta)_{stable} = C\sin(\theta)\exp[-Z(\theta - \theta_o)^2]$; $P(\theta)_{dispers} = C\sin(\theta)\exp[-k\theta^2]$; where C is a scaling constant used to produce distributions of approximately equal height, and $k = 1/[1/Z + 2\langle\theta^2\rangle]$. (*A*) $Z = 1.0$ (representing an RNA chain of ~200–250 bp); (*B*) $Z = 4.0$; (*C*) rigid case. Note that although the distributions are given in degrees, the above expressions utilize angles in radians. The corresponding TEB decay curves for each case are displayed in *D*, *E*, and *F*, respectively. The curves were generated from tabulated amplitude and decay time data presented by Roitman and Zimm (1984b; Roitman, 1984).

CONCLUSIONS

The current investigation has demonstrated that Brownian dynamics simulations are capable of accurately describing both the τ-ratios and fractional amplitudes associated with the birefringence decay profiles of RNA molecules possessing central bends. The τ-ratios derived from the current simulations are nearly identical to the corresponding τ-ratios determined from the equilibrium-ensemble approach, indicating that either method can be used for the purpose of obtaining ensemble-average (mean) angles for bends associated with various nonhelix elements in RNA (or DNA). Moreover, the current simulations predict a correlation between bend angles and the fractional (slow) amplitudes for bulge-containing RNA molecules that is in good agreement with previous experimental observations (Zacharias and Hagerman, 1995a).

A more detailed Brownian dynamics analysis of molecules with central bends of variable dispersive character reveals that the distinction between stable and dispersive bends is quite subtle; a clear distinction between stable and dispersive bends generally cannot be made on the basis of single TEB measurements, particularly for molecules of ~150 bp or greater; additional defining measurements are required. The similar behavior for stable and dispersive bends derives from the fact that the terminal decay behavior is determined largely by the ensemble-average properties of the chain, an observation that was made originally by Roitman and Zimm (1984a,b; Roitman, 1984; see also Allison and Nambi, 1992). However, the current analysis also indicates that under certain circumstances (i.e., apparent angles less than ~80°; sufficiently short/stiff molecules), the fractional amplitudes may reveal differences between stable and highly flexible bends.

The authors thank Drs. Daniel Roitman and Bruno Zimm for useful discussions.

This work was supported by a grant from the National Institutes of Health (GM 35305 to PJH) and by a habililation grant (to MZ) from the Deutsche Forschungsgemeinschaft.

REFERENCES

Allison, S. A., and J. A. McCammon. 1984. Transport properties of rigid and flexible macromolecules by Brownian dynamics simulation. *Biopolymers.* 23:167–187.

Allison, S. A., and P. Nambi. 1992. Electric dichroism and birefringence decay of short DNA restriction fragments studied by Brownian dynamics simulation. *Macromolecules.* 25:759–768.

Amiri, K. M. A., and P. J. Hagerman. 1994. Global structure of a self-cleaving hammerhead RNA. *Biochemistry.* 33:13172–13177.

Amiri, K. M. A., and P. J. Hagerman. 1996. The global conformation of an active hammerhead RNA during the process of self-cleavage. *J. Mol. Biol.* 261:125–134.

Antosiewicz, J., and J. A. McCammon. 1995. Electrostatic and hydrodynamic orientational steering effects in enzyme substrate association. *Biophys. J.* 69:57–65.

Bloomfield, V. A., D. M. Crothers, and I. Tinoco. 1974. Physical Chemistry of Nucleic Acids. Harper and Row, New York.

Chirico, G., and J. Langowski. 1994. Kinetics of DNA supercoiling studied by Brownian dynamics simulation. *Biopolymers.* 34:415–433.

Diekmann, S., W. Hillen, B. Morgeneyer, R. D. Wells, and D. Porschke. 1982. Orientation relaxation of DNA restriction fragments and the internal mobility of the double helix. *Biophys. Chem.* 15:263–270.

Eis, P. S., and D. P. Millar. 1993. Conformational distributions of a four-way DNA junction revealed by time-resolved fluorescence resonance energy transfer. *Biochemistry.* 32:13852–13860.

Elias, J. G., and D. Eden. 1981. Transient electric birefringence study of the persistence length and electric polarizability of restriction fragments in DNA. *Macromolecules.* 14:410–419.

Ermak, D. L., and J. A. McCammon. 1978. Brownian dynamics with hydrodynamic interactions. *J. Chem. Phys.* 69:1352–1360.

Fixman, M. 1978a. Simulation of polymer dynamics. I. General theory. *J. Chem. Phys.* 69:1527–1537.

Fixman, M. 1978b. Simulation of polymer dynamics. II. Relaxation rates and dynamic viscosity. *J. Chem. Phys.* 69:1538–1545.

Friederich, M. W., F.-U. Gast, E. Vacano, and P. J. Hagerman. 1995. Determination of the angle between the anticodon and aminoacyl acceptor stems of yeast phenylalanyl tRNA in solution. *Proc. Natl. Acad. Sci. USA.* 92:4803–4807.

Gast, F.-U., K. M. A. Amiri, and P. J. Hagerman. 1994. Interhelix geometry of stems I and II of a self-cleaving hammerhead RNA. *Biochemistry.* 33:1788–1796.

Gast, F.-U., and P. J. Hagerman. 1991. Electrophoretic and hydrodynamic properties of duplex ribonucleic acid molecules transcribed in vitro: evidence that A-tracts do not generate curvature in RNA. *Biochemistry.* 30:4268–4277.

Grycuk, T., J. Antosiewicz, and D. Porschke. 1994. Brownian dynamics of the polarization of rodlike polyelectrolytes. *J. Phys. Chem.* 98: 10881–10887.

Hagerman, K. R., and P. J. Hagerman. 1996. Helix rigidity of DNA: the meroduplex as an experimental paradigm. *J. Mol. Biol.* 260:207–223.

Hagerman, P. J. 1981. Investigation of the flexibility of DNA using transient electric birefringence. *Biopolymers.* 20:1503–1535.

Hagerman, P. J. 1996. "Sometimes a great motion": the application of transient electric birefringence to the study of macromolecular structure. *Curr. Opin. Struct. Biol.* 6:643–649.

Hagerman, P. J., and B. Zimm. 1981. Monte Carlo approach to the analysis of the rotational diffusion of wormlike chains. *Biopolymers.* 20: 1481–1502.

IMSL. 1980. IMSL Library 3 Reference Manual, IMSL LIB3-0005. International Mathematical and Statistical Libraries, Houston, TX.

Kebbekus, P., D. E. Draper, and P. Hagerman. 1995. Persistence length of RNA. *Biochemistry.* 34:4354–4357.

Lewis, R. J., S. A. Allison, D. Eden, and R. Pecora. 1988. Brownian dynamics simulations of a three-subunit and a ten-subunit worm-like chain: comparison of results with trumbell theory and with experimental results from DNA. *J. Chem. Phys.* 89:2490–2503.

Lewis, R. J., R. Pecora, and D. Eden. 1986. Transient electric birefringence measurements of the rotational and internal bending modes in monodisperse DNA fragments. *Macromolecules.* 19:134–139.

Luty, B. A., R. C. Wade, J. D. Madura, and J. A. McCammon. 1993. Brownian dynamics simulations of diffusional encounters between triose phosphate isomerase and glyceraldehyde phosphate: electrostatic steering of glyceraldehyde phosphate. *J. Phys. Chem.* 97:233–237.

Mellado, P., A. Iniesta, F. G. Diaz, and J. Garcia de la Torre. 1988. Diffusion coefficients of segmentally flexible macromolecules with two subunits: a study of broken rods. *Biopolymers.* 27:1771–1786.

Northrup, S. H., S. A. Allison, and J. A. McCammon. 1984. Brownian dynamics simulation of diffusion-influence biomolecular reactions. *J. Phys. Chem.* 80:1517–1524.

Press, W. H., W. T. Vetterling, S. A. Teukolsky, and B. P. Flannery. 1992. Numerical Recipes in Fortran: The Art of Scientific Computing. Cambridge University Press, Cambridge, England. 678–683.

Roitman, D. B. 1984. an elastic hinge model for dynamics of stiff chains. III. Viscoelastic and Kerr-effect behavior of bent molecules. *J. Chem. Phys.* 81:6356–6360.

Roitman, D. B., and B. Zimm. 1984a. An elastic hinge model for dynamics of stiff chains. I. Viscoelastic properties. *J. Chem. Phys.* 81:6340–6347.

Roitman, D. B., and B. Zimm. 1984b. An elastic hinge model for dynamics of stiff chains. II. Transient electro-optical properties. *J. Chem. Phys.* 81:6348–6354.

Rose, M. E. 1957. Elementary Theory of Angular Momentum. Wiley, New York.

Rotne, J., and S. Prager. 1969. Variational treatment of hydrodynamic interactions in polymers. *J. Chem. Phys.* 50:4831–4837.

Ryckaert, J. P., G. Ciccoti, and H. J. C. Berendsen. 1977. Molecular dynamics of liquid alkanes. *J. Comp. Phys.* 23:327–341.

Sharp, K., R. Fine, and B. Honig. 1987. Computer simulation of a substrate to an active site of an enzyme. *Science.* 236:1460–1463.

Shen, Z., and P. J. Hagerman. 1994. Geometry of the central branch of the 5S ribosomal RNA of *Sulfolobus acidocaldarius. J. Mol. Biol.* 241: 415–430.

Stellwagen, N. C. 1981. Electric birefringence of restriction enzyme fragments of DNA: optical factor and electric polarizability as a function of molecular weight. *Biopolymers.* 29:399–434.

Vacano, E., and P. J. Hagerman. 1997. Analysis of birefringence decay profiles for nucleic acid helices possessing bends or regions of increased flexibility: the τ-ratio approach. *Biophys. J.* 73:306–317.

Wegener, W. A. 1986. Transient electric birefringence of dilute rigid-body suspensions at low field strength. *J. Chem. Phys.* 84:5989–6004.

Wegener, W. A., R. M. Dowben, and V. J. Koester. 1979. Time-dependent birefringence, linear dichroism, and optical rotation resulting from rigid body rotational diffusion. *J. Chem. Phys.* 70:622–632.

Zacharias, M., and P. J. Hagerman. 1995a. Bulge-induced bends in RNA: quantification by transient electric birefringence. *J. Mol. Biol.* 247: 486–500.

Zacharias, M., and P. J. Hagerman. 1995b. The bend in RNA created by the trans-activation response element bulge of human immunodeficiency virus is straightened by arginine and by Tat-derived peptide. *Proc. Natl. Acad. Sci. USA.* 92:6052–6056.

Zacharias, M., and P. J. Hagerman. 1996. The influence of symmetric internal loops on the flexibility of RNA. *J. Mol. Biol.* 257:276–289.